



Enantiomer detection via quantum Otto cycleMohsen Izadyari ^{1,*}, M. Tahir Naseem,^{1,†} and Özgür E. Müstecaplıoğlu ^{1,2,‡}¹*Department of Physics, Koç University, 34450 Sarıyer, Istanbul, Türkiye*²*TÜBİTAK Research Institute for Fundamental Sciences, 41470 Gebze, Türkiye*

(Received 30 November 2022; accepted 11 April 2023; published 26 April 2023)

Enantiomers are chiral molecules that exist in right-handed and left-handed conformations. Optical techniques of enantiomers' detection are widely employed to discriminate between left- and right-handed molecules. However, identical spectra of enantiomers make enantiomer detection a very challenging task. Here, we investigate the possibility of exploiting thermodynamic processes for enantiomer detection. In particular, we employ a quantum Otto cycle in which a chiral molecule described by a three-level system with cyclic optical transitions is considered a working medium. Each energy transition of the three-level system is coupled with an external laser drive. We find that the left- and right-handed enantiomers operate as a quantum heat engine and a thermal accelerator, respectively, when the overall phase is the control parameter. In addition, both enantiomers act as heat engines by keeping the overall phase constant and using the laser drives' detuning as the control parameter during the cycle. However, the molecules can still be distinguished because both cases' extracted work and efficiency are quantitatively very different. Accordingly, the left- and right-handed molecules can be distinguished by evaluating the work distribution in the Otto cycle.

DOI: [10.1103/PhysRevE.107.L042103](https://doi.org/10.1103/PhysRevE.107.L042103)**I. INTRODUCTION**

Quantum thermodynamics investigates the applicability of laws of thermodynamics and their possible generalizations in the realm of quantum mechanics [1–7]. At variance to macroscopic heat engines, in both stochastic [8–11] and quantum heat engines [7,12], fluctuations become nonnegligible when the typical energy scales are comparable to $k_B T$. The concept of utilizing thermodynamics to infer the characteristics of a system has been discussed within stochastic thermodynamics, specifically in relation to the thermodynamic uncertainty relations [13]. Furthermore, quantum heat engines (QHEs) serve as test beds for fundamental discussions and practical applications of quantum thermodynamics [7]. QHEs were implemented recently employing different physical setups, such as nitrogen-vacancy centers [14], the spin-1/2 working medium [15,16], and a single-ion system [17]. Further, the measurement of thermodynamical quantities like work and heat in the quantum context attracted attention recently [18–23]. For instance, to measure work in closed quantum systems, a single projective measurement [24,25] and two-time measurement [26] methods were proposed. The reservoir(s) energy is not conserved in open quantum systems, and although there are open questions about the definition and experimental measurements of work and heat [27,28], some methods were reported in the context of quantum stochastic thermodynamics [29]. In a broad context, QHE is a thermal machine whose operation cycle requires a quantum mechani-

cal description. A typical example is the quantum Otto cycle (QOC), where the fast isentropic compression and expansion strokes of its classical counterpart are replaced by the slow quantum adiabatic parametric processes [12,30–33]. Different quantum working substances were proposed to implement QOC [34–39] and experimental demonstrations were reported for spin systems [16,26,40]. These studies revealed that a QOC's work output and efficiency are determined by the energy spectrum of the quantum working system. Accordingly, we ask if a QOC can be used as a probe to discriminate systems with identical energy spectrums but with distinct spectral changes under the same parametric processes. A specific system with such a spectral character and for which this question is particularly significant is a chiral molecule.

Chiral molecules can have either left- or right-handed geometries that are not superimposable on their mirror images [41,42]. They play a significant role in fundamentals and applications in biology [43–45], physics [46], and pharmacology [47]. The two mirror-image molecules are called enantiomers. Enantiomers exhibit identical physical and chemical properties in an achiral environment, while they can act remarkably differently when placed in a chiral environment [45]. Chiral molecules may exist as a mixture of enantiomers in varying proportions. Therefore, enantioseparation is a critical and challenging task in chemistry and medicine [48–54].

Optical enantio-separation techniques are one of the most common methods for enantio-detection based on the interference between the electric and the magnetic dipole transitions [50,54]. Enantiomer-specific microwave spectroscopic methods, based on cyclic three-level systems, which can exist in chiral molecules [55,56] and other artificial symmetry-broken systems [57], were examined for the enantio-detection of chiral molecules [55,58–63]. Three-level quantum systems

*mizadyari18@ku.edu.tr

†mnaseem16@ku.edu.tr

‡omustecap@ku.edu.tr

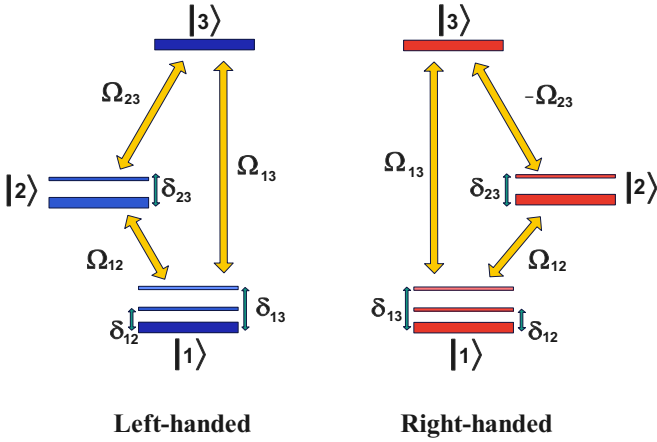


FIG. 1. A schematic illustration of a left-handed and right-handed chiral molecule. The three-level system is coupled with three classical optical drives of Rabi frequencies Ω_{12} , Ω_{13} , and $\pm\Omega_{23}$, where $+\Omega_{23}$ ($-\Omega_{23}$) describes the left-handed (right-handed) molecule. The detunings of the external optical drives from energy transitions are indicated by δ_{ij} .

with broken symmetry allow the coexistence of one- and two-photon transitions such that a cyclic population transfer can occur between different energy levels [55,56,64–66]. In this Letter, we consider a chiral molecule, described by a three-level system with cyclic optical transitions, as our working substance subject to a QOC. By calculating the work and efficiency of the engine, we investigate if left- and right-handed enantiomers can have different energetics that can be probed by the engine’s behavior and performance.

The rest of the Letter is organized as follows. In Sec. II, we describe and shortly review the Hamiltonian model to describe a cyclic three-level chiral molecule. We introduce the QOC operation in Sec. III. To discriminate the enantiomers, quantum thermodynamic work and efficiency are calculated in Sec. IV. We present a summary of the work in Sec. V.

II. MODEL SYSTEM

We consider a chiral molecule described by a three-level system with cyclic optical transitions driven by three classical optical fields [55,56,67], which is shown in Fig. 1. The physical mechanism of the system stems from the Hamiltonian of an asymmetric top in an external electric field [63,68]. The implementation of cyclic three-level configurations, as a means of describing chiral molecules through molecular rotation, was investigated in Ref. [56], thereby demonstrating the proposal’s viability. The Hamiltonian of this system in the rotating wave approximation is given by [55,56,67]

$$H = \sum_{j=1}^3 \omega_j |j\rangle + \sum_{i>j=1}^3 [\Omega_{ij}(t)e^{-i\omega_{ij}t} |i\rangle \langle j| + \text{H.c.}] \quad (1)$$

Here, the first term describes the energy of a three-level system with ω_j being the energy of the state $|j\rangle$. The second term describes the coupling of classical optical fields with the three-level atom; the frequency of the optical field is given by ω_{ij} which describes the coupling between $|i\rangle \leftrightarrow |j\rangle$ energy levels.

$\Omega_{ij}(t) = \bar{\mu}_{ij} \cdot \vec{E}_{ij}$ represents the Rabi frequency which depends on the field strength \vec{E}_{ij} and associated transition dipole matrix element $\bar{\mu}_{ij}$ between the states $|i\rangle$ and $|j\rangle$. To confirm that each transition’s dynamics can influence the three-level process’s global dynamics, the three Rabi frequencies must be comparable. This can be achieved by adjusting the intensities of microwave fields and/or selecting the level spacing judiciously [56]. Enantio-selective excitation with three pulses was experimentally demonstrated in microwave three-wave mixing experiments [62,69–71]. Furthermore, a method to impart a nonzero overall phase was introduced in Ref. [67]. In the interaction picture, the Hamiltonian of the chiral molecule is given by

$$H_{\text{int}}^{\pm} = \begin{pmatrix} \delta_{13} & \Omega_{12}e^{i(\Delta t + \Phi)} & \Omega_{13} \\ \Omega_{12}e^{-i(\Delta t + \Phi)} & \delta_{23} & \pm\Omega_{23} \\ \Omega_{13} & \pm\Omega_{23} & 0 \end{pmatrix}. \quad (2)$$

Here, δ_{ij} is the detuning of the optical fields with energy levels $|i\rangle \leftrightarrow |j\rangle$ and $\Delta := \delta_{12} - \delta_{13} + \delta_{23}$. In addition, we define the overall phase $\Phi := \Phi_{12} - \Phi_{13} + \Phi_{23}$, where $\Phi_{ij} = \phi_{ij} + \theta_{ij}$ contains the material phase θ_{ij} and the phases of the electric fields ϕ_{ij} [67]. The interference of one-photon and two-photon processes results in a sign change in the product of the three Rabi frequencies, which is attributed to the system’s chirality dependency [56]. We stress that the difference between the left- and right-handed molecules are expressed by the $\pm\Omega_{23}$, where the left-handed and right-handed molecules are given by positive and negative Rabi frequency Ω_{23} , respectively (see Fig. 1).

According to Eq. (2), the interaction Hamiltonian becomes time-independent for $\Delta = 0$ [67]. In the rest of the Letter, we assume $\delta_{12} = \delta_{23} = \delta_{13}/2 \equiv \delta$ for which Δ becomes zero and the Hamiltonian becomes time independent. This can be achieved by making a judicious choice on the selection of frequencies ω_{ij} . All system parameters can be scaled for convenience with arbitrary energy E_0 . Henceforth, we assume that the system parameters are scaled with rotational energy $E_0 = \hbar B$, defined by the angular momentum operators concerning the principle molecular axes [67], with the rotational constant B (i.e., for menthol $B \approx 692$ MHz) [67]. Accordingly, time and frequencies are given in units of $\tau_0 = \hbar/E_0$ and $1/\tau_0$.

Figure 2 displays the eigenvalues of the Hamiltonian H^{\pm} given in Eq. (2) as a function of the overall phase Φ and detuning δ . We implement the adiabatic strokes in the QOC by either varying the overall phase Φ or detuning δ ; the adiabaticity condition requires no level crossing of the energy levels of the working medium. This is why we consider the system parameters in Fig. 2 and the rest of the Letter such that there is no level crossing in the field-dressed eigenstates, which can occur for $\Phi = 0, \pi, 2\pi$, and $\delta = 0$ [67]. According to Figs. 2(c) and 2(d), the left- and right-handed enantiomers have identical energy spectrums for phases $\Phi = \pi/2$ and $\Phi = 3\pi/2$. We consider these two-phase values as the starting and ending points of the adiabatic strokes in the cycle in Sec. IV A. Although the energy spectrum is identical at the start and end of the adiabatic strokes, we will show that the Otto cycle discriminates the left- and right-handed enantiomer in the output work. Furthermore, we investigate the Otto cycle

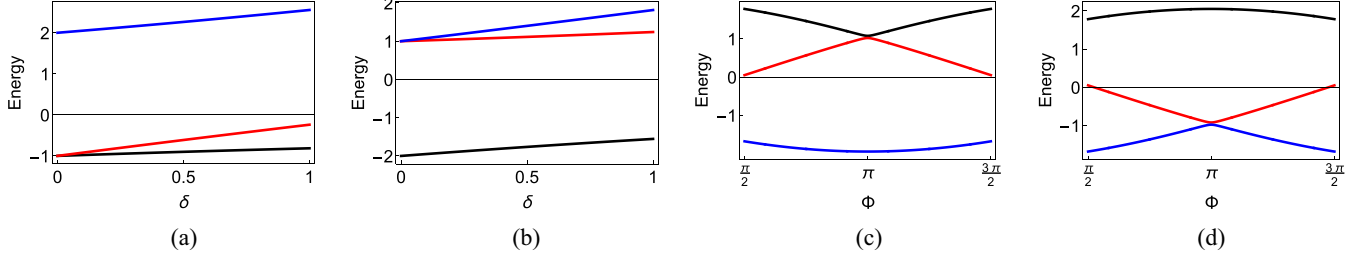


FIG. 2. Energy eigenvalues of the Hamiltonian H_{int}^{\pm} for [(a), (b)] constant overall phase $\Phi = 0$ and [(c), (d)] constant detuning $\delta = 0.1/\tau_0$. The panels [(a), (c)] and [(b), (d)] represent left- and right-handed enantiomers, respectively. The eigenenergies are scaled with the rotational energy $E_0 = \hbar B$ with the rotational constant B , that is why eigenenergies are $\pm 1E_0$ and $\pm 2E_0$ for $\Phi = \delta = 0$. The eigenvalues are obtained for time-independent Hamiltonian ($\Delta = 0$) and considering the unit magnitude of the Rabi frequencies Ω_{ij} .

by keeping the overall phase constant and adjusting the detuning in adiabatic processes as a more practical assumption in Sec. IV B.

III. CHIRAL MOLECULE OTTO CYCLE

A QOC consists of two quantum isochoric and two adiabatic processes [72]. We consider a chiral three-level system with cyclic optical transitions as a working medium of our QOC. The system in the QOC is in contact with a hot and cold bath in two isochoric processes. During the adiabatic strokes of the cycle, the Hamiltonian changes slowly and the system is not allowed to exchange heat with the environment. At the start of the cycle, we assume that the working medium is in thermal equilibrium with the cold thermal bath of inverse temperature β_c . The four strokes of the QOC are described as follows.

A. Hot isochore ($A \rightarrow B$)

The first stroke is the quantum isochoric heating process in which the working medium is coupled to a hot bath of inverse temperature β_h . During this stroke, Q_h heat is injected into the system; the Hamiltonian H_{int}^{\pm} is kept constant, and accordingly, no work is done. At the end of this stroke, we assume that the working medium comes to equilibrium with the hot thermal bath and each energy level has an occupation probability of $P_j(\beta_h)$. To show the validity of the thermalization assumption, we present numerical simulations of a three-level system coupled to a thermal bath in the presence of external drives in the Supplemental Material [73]. The exchanged heat Q_h with the hot thermal bath is calculated by [79]

$$Q_h = \sum_{n=1}^3 E_n(A)[P_n(\beta_h) - P_n(\beta_c)]. \quad (3)$$

Here, $E_n(A)$ is n th eigenenergy of system Hamiltonian H_{int} for overall phase Φ_1 and the population of the associated eigenstate is changed from $P_n(\beta_c)$ to $P_n(\beta_h)$.

B. Adiabatic expansion ($B \rightarrow C$)

During this stage, the system is decoupled from the hot bath and the system Hamiltonian is changed from $H(A)$ to $H(B)$. We discuss two strategies to implement the adiabatic strokes. First, varying Φ from Φ_1 to Φ_2 by keeping detuning

constant such that $\delta > 0$. In the second case, changing the detuning δ from δ_1 to δ_2 for constant phase Φ . Work is extracted from the system during this stage of the cycle. We assume this process is slow enough that the occupation probabilities of the energy levels are unchanged to satisfy the adiabaticity condition [80].

C. Cold isochore ($C \rightarrow D$)

During this stage, the system is subject to either constant phase Φ and it is put into contact with the cold bath of inverse temperature β_c for a time τ_c . The exchanged heat between the system and the cold bath is given by

$$Q_c = \sum_{n=1}^3 E_n(B)[P_n(\beta_c) - P_n(\beta_h)]. \quad (4)$$

At point D , the system reaches to a thermal state defined by inverse temperature β_c and no work is done during this stage.

D. Adiabatic compression ($D \rightarrow A$)

Similar to adiabatic expansion, the system is isolated from the environment during this stage. The eigenenergies are changed by varying either phase Φ or detuning δ ; the occupation probabilities remain the same during this stroke. The net produced work during a cycle can be calculated by using Eqs. (3) and (4)

$$\begin{aligned} W_0 &= Q_h + Q_c \\ &= \sum_{n=1}^3 [E_n(A) - E_n(B)][P_n(\beta_h) - P_n(\beta_c)]. \end{aligned} \quad (5)$$

The efficiency of a heat engine is defined as $\eta = W_0/Q_h$. Here we adopt the convention that the work done on (by) the system is positive and the heat flow out of (into) the system is negative.

For a possible experimental realization of the proposed model, a laser cooling beam at temperature T_c can be employed to create an equilibrium cold bath [17], while white noise from an electric field can serve as the hot bath [7]. A cyclic three-level system immersed in a thermal bath reaches a fully thermalized steady state [81]. Full thermalization with the hot bath enables the utilization of the interferometric method to characterize the output work, as was demonstrated in previous studies [16,82,83]. Specifically, the characteristic

function of the work probability distribution can be measured, yielding the mean value of the extracted work [16,84]. Additionally, quantum-state tomography procedures can be conducted at the beginning and end of the energy gap compression and expansion strokes to measure the heat absorbed from the hot bath [16]. By measuring the output work and heat absorbed from the hot bath, the quantum heat engine can be fully characterized.

IV. RESULTS

We look for the signatures in the work output of the Otto cycle to distinguish left- and right-handed enantiomers. The system's Hamiltonian [Eq. (2)] is a function of the overall phase Φ and detuning δ . As a result, the adiabatic stages of the cycle can be implemented either by varying the phase or detuning and keeping the other constant during the stroke. In this section, we examine both strategies for implementing the Otto cycle and evaluate the output work to distinguish enantiomers. First, we investigate the Otto cycle in constant detuning δ regime while the overall phase employs as the control parameter in Sec. IV A, then in Sec. IV B we examine the Otto cycle when δ is the control parameter and the overall phase is kept constant.

A. Control parameter Φ

We adhere to the sign conventions of absorbed (rejected) heat is positive (negative) and the work extracted (consumed) is negative. Accordingly, the thermal machines' operations can be categorized into four distinct regimes [85]

Engine :	$W \leq 0, Q_h \geq 0, Q_c \leq 0,$
Refrigerator :	$W \geq 0, Q_h \leq 0, Q_c \geq 0,$
Heater :	$W \geq 0, Q_h \leq 0, Q_c \leq 0,$
Thermal accelerator :	$W \geq 0, Q_h \geq 0, Q_c \leq 0.$

We consider the set of system parameters for which there is no level crossing between the energy levels during the Otto cycle (see Fig. 2). Accordingly, we consider the phase $\Phi_1 = \pi/2$ at the start of the adiabatic expansion and change it to $\Phi_2 = 3\pi/2$ at the end of this stage. Similarly, the phase is changed from Φ_2 to Φ_1 in the adiabatic compression stage. During the adiabatic stages' detuning $\delta = 0.1/\tau_0$ is kept constant. The heat exchanged with the thermal baths and extracted work for left- and right-handed systems are shown in Fig. 3. For both left- and right-handed enantiomers, the heat injected Q_h from the hot bath into the system is positive and the heat rejected Q_c into the cold bath is negative. However, the work distribution reveals that work is extracted from the left-handed system ($W < 0$), but in the right-handed system, the work is done on the system ($W > 0$). Accordingly, the left- and right-handed enantiomers operate as the heat engine and the thermal accelerator, respectively. Therefore, the thermodynamic responses of the enantiomers are not the same, which can be used as a probe to distinguish these enantiomers.

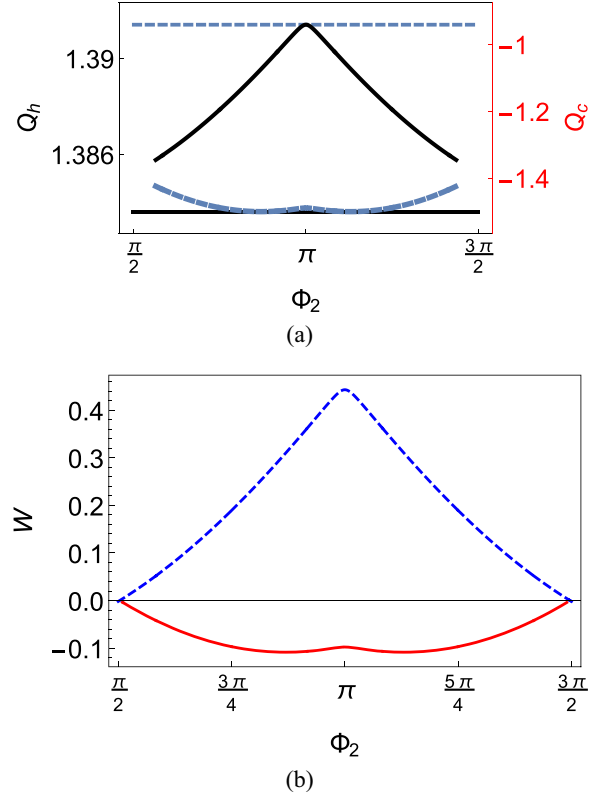


FIG. 3. (a) Heat exchange Q_h with the hot bath and Q_c (scaled by $E_0 = \hbar B$) with the cold bath as a function of the overall phase Φ of the optical drives with constant $\delta = 0.1/\tau_0$. The hot and cold baths have inverse temperatures $\beta_h = 0.01$ and $\beta_c = 1$, respectively. The solid and dashed lines are for the right- and left-handed enantiomers. In addition, the upper and lower horizontal lines represent heat Q_h injected into the system and the heat rejected Q_c into the cold bath is denoted by curved lines. (b) Work output W as a function of the phase Φ of the optical drives in the QOC. The solid and dashed lines are for the left- and right-handed enantiomers, respectively. In SI units the system parameters are given by $E_0 = \hbar B = 2\pi \hbar 692 \times 10^6 = 0.033$, $T_h = 3.3$ K, and $T_c = 0.033$ K. At these system parameters the energy scale of the system is comparable with the thermal energy $k_B T$, which indicates that validity of our analysis in the quantum regime.

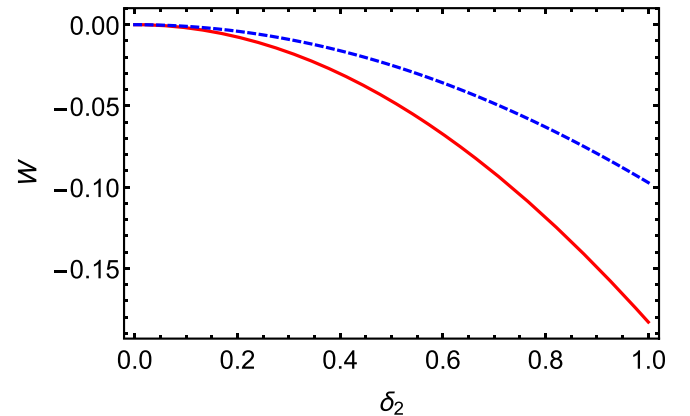


FIG. 4. Work output W as a function of the detuning δ_2 (scaled by τ_0) supposing the optical drive fixed initially at resonance $\delta_1 = 0$ and overall phase kept constant at $\Phi = 0$. The hot and cold baths have inverse temperatures $\beta_h = 0.01$ and $\beta_c = 1$, respectively. The solid and dashed lines are for the left- and right-handed enantiomers.

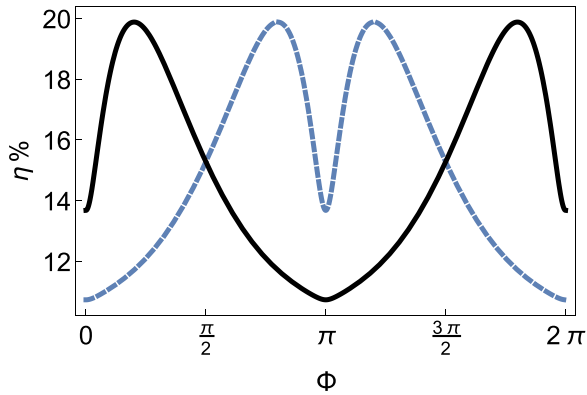


FIG. 5. The engine's efficiency $\eta(\%)$ as a function of Φ , while detuning as a control parameter modifies from $\delta = 0$ to $\delta = 1/\tau_0$. The hot and cold baths have inverse temperatures $\beta_h = 0.01$ and $\beta_c = 1$, respectively. The solid and dashed lines are for the left- and right-handed Otto engines.

B. Control parameter δ

It can be of practical importance to check the thermal behaviors of chiral three-level systems in the Otto cycle using δ as the control parameter with a constant phase Φ . The work output, in this case, is shown in Fig. 4, which shows that both the left- and right-handed enantiomers operate as heat engines. However, the extracted work in both cases can be significantly different. The extracted work differs between left- and right-handed systems based on the constant Φ selection. For instance, if we keep overall phase $\Phi = \pi/2$ during the Otto cycle, the obtained extracted work is the same for both enantiomers, but it is significantly different for $\Phi = \pi$ where $W_{\text{left}} = -0.18 E_0$ and $W_{\text{right}} = -0.097 E_0$.

The efficiency of the Otto engine is given by

$$\eta(\%) = \frac{|W|}{Q_h} \times 100. \quad (6)$$

To study the efficiency, we consider the control parameter δ modifying from $\delta_1 = 0$ to $\delta_2 = 1/\tau_0$. We define the efficiency as a function of the overall phase Φ , which is constant during the cycle. The engine's efficiency corresponds to Φ is plotted in Fig. 5 where the solid black and dashed blue curves denote the left- and right-handed system's efficiency, respectively.

According to Fig. 5, the magnitude of maximum efficiency for both cases is the same, $\eta \approx 20\%$. The curves intersect, so both are equally efficient in a particular Φ . However, their efficiency is distinct at other Φ values. For example, the left-handed Otto engine's maximum efficiency is obtained at $\Phi \approx \pi/5$, and $6\pi/5$ while it is maximum at $\Phi \approx \pi \pm 0.7$ for the right-handed engine. Also, $\eta_{\text{left}} = \eta_{\text{right}}$ at $\Phi = \pi/2$ and $3\pi/2$ which comes from their identical energy spectrum in these points (Fig. 2). Therefore, one enantiomer may be more favorable for some energy processes because of its distinguishing efficiency, even if it can perform the same energetic function (such as operating a heat engine).

V. CONCLUSION

In this Letter, we investigated the possibility of exploiting thermodynamic processes for enantiomers' detection. In particular, we considered a chiral molecule described by a cyclic three-level system coupled to three external classical optical fields. We found that, depending on the phase and detuning of the optical fields, the left- and right-handed cyclic three-level system exhibited different thermal signatures when subjected to an Otto cycle. In addition to the practical distinction of enantiomers, our results fundamentally suggest that different enantiomers may be associated with different thermodynamic (energetic) functions in chemical or biological processes, such as work harvesting. In addition, even if they are capable of performing the same energetic function, their efficiencies may differ so that one enantiomer may be more favorable than the other.

Enantiomer detection is a formidable task, even for the case of two enantiomers, because of their identical energy spectra [67,86,87]. Our method of enantiomer detection via work distribution can be an alternative to more widely employed schemes for discrimination between the enantiomers [50,54].

ACKNOWLEDGMENTS

This work was supported by the Scientific and Technological Research Council of Türkiye (TÜBİTAK) with Project No. 120F089. The authors thank Dr. Onur Pusuluk for the helpful discussions.

- [1] G. J., M. Micheal, and G. Mahler, *Quantum Thermodynamics* (Oxford University Press, New York, 2007).
- [2] R. Kosloff, Quantum thermodynamics: A dynamical viewpoint, *Entropy* **15**, 2100 (2013).
- [3] S. Vinjanampathy and J. Anders, Quantum thermodynamics, *Contemp. Phys.* **57**, 545 (2016).
- [4] J. Goold, M. Huber, A. Riera, L. del Rio, and P. Skrzypczyk, The role of quantum information in thermodynamics: a topical review, *J. Phys. A: Math. Theor.* **49**, 143001 (2016).
- [5] S. Deffner and S. Campbell, *Quantum Thermodynamics* (Morgan Claypool Publishers, 2019), pp. 2053–2571.
- [6] A. Tuncer and Ö. E. Müstecaplıoğlu, Quantum thermodynamics and quantum coherence engines, *Turk. J. Phys.* **44**, 404 (2020).
- [7] N. M. Myers, O. Abah, and S. Deffner, Quantum thermodynamic devices: From theoretical proposals to experimental reality, *AVS Quantum Science* **4**, 027101 (2022).
- [8] T. Schmiedl and U. Seifert, Efficiency at maximum power: An analytically solvable model for stochastic heat engines, *Europhys. Lett.* **81**, 20003 (2008).
- [9] V. Blickle and C. Bechinger, Realization of a micrometre-sized stochastic heat engine, *Nat. Phys.* **8**, 143 (2012).
- [10] S. Krishnamurthy, S. Ghosh, D. Chatterji, R. Ganapathy, and A. K. Sood, A micrometre-sized heat engine operating between bacterial reservoirs, *Nat. Phys.* **12**, 1134 (2016).
- [11] A. Datta, P. Pietzonka, and A. C. Barato, Second Law for Active Heat Engines, *Phys. Rev. X* **12**, 031034 (2022).

- [12] R. Kosloff and A. Levy, Quantum heat engines and refrigerators: Continuous devices, *Annu. Rev. Phys. Chem.* **65**, 365 (2014).
- [13] U. Seifert, From stochastic thermodynamics to thermodynamic inference, *Annu. Rev. Condens. Matter Phys.* **10**, 171 (2019).
- [14] J. Klatzow, J. N. Becker, P. M. Ledingham, C. Weinzetl, K. T. Kaczmarek, D. J. Saunders, J. Nunn, I. A. Walmsley, R. Uzdin, and E. Poem, Experimental Demonstration of Quantum Effects in the Operation of Microscopic Heat Engines, *Phys. Rev. Lett.* **122**, 110601 (2019).
- [15] R. J. de Assis, T. M. de Mendonca, C. J. Villas-Boas, A. M. de Souza, R. S. Sarthour, I. S. Oliveira, and N. G. de Almeida, Efficiency of a Quantum Otto Heat Engine Operating under a Reservoir at Effective Negative Temperatures, *Phys. Rev. Lett.* **122**, 240602 (2019).
- [16] J. P. S. Peterson, T. B. Batalhão, M. Herrera, A. M. Souza, R. S. Sarthour, I. S. Oliveira, and R. M. Serra, Experimental Characterization of a Spin Quantum Heat Engine, *Phys. Rev. Lett.* **123**, 240601 (2019).
- [17] J. Roßnagel, S. T. Dawkins, K. N. Tolazzi, O. Abah, E. Lutz, F. Schmidt-Kaler, and K. Singer, A single-atom heat engine, *Science* **352**, 325 (2016).
- [18] M. Campisi, R. Blattmann, S. Kohler, D. Zueco, and P. Hänggi, Employing circuit qed to measure non-equilibrium work fluctuations, *New J. Phys.* **15**, 105028 (2013).
- [19] P. Smacchia and A. Silva, Work distribution and edge singularities for generic time-dependent protocols in extended systems, *Phys. Rev. E* **88**, 042109 (2013).
- [20] O. P. Saira, Y. Yoon, T. Tanttu, M. Mottonen, D. V. Averin, and J. P. Pekola, Test of the Jarzynski and Crooks Fluctuation Relations in an Electronic System, *Phys. Rev. Lett.* **109**, 180601 (2012).
- [21] T. B. Batalhao, A. M. Souza, L. Mazzola, R. Aucaisse, R. S. Sarthour, I. S. Oliveira, J. Goold, G. De Chiara, M. Paternostro, and R. M. Serra, Experimental Reconstruction of Work Distribution and Study of Fluctuation Relations in a Closed Quantum System, *Phys. Rev. Lett.* **113**, 140601 (2014).
- [22] S. An, J. Zhang, M. Um, D. Lv, Y. Lu, J. Zhang, Z. Yin, H. T. Quan, and K. Kim, Experimental test of the quantum jarzynski equality with a trapped-ion system, *Nat. Phys.* **11**, 193 (2015).
- [23] L. Fusco, S. Pigeon, T. J. G. Apollaro, A. Xuereb, L. Mazzola, M. Campisi, A. Ferraro, M. Paternostro, and G. De Chiara, Assessing the Nonequilibrium Thermodynamics in a Quenched Quantum Many-Body System via Single Projective Measurements, *Phys. Rev. X* **4**, 031029 (2014).
- [24] A. J. Roncaglia, F. Cerisola, and J. P. Paz, Work Measurement as a Generalized Quantum Measurement, *Phys. Rev. Lett.* **113**, 250601 (2014).
- [25] G. De Chiara, A. J. Roncaglia, and J. P. Paz, Measuring work and heat in ultracold quantum gases, *New J. Phys.* **17**, 035004 (2015).
- [26] Q. Bouton, J. Nettersheim, S. Burgardt, D. Adam, E. Lutz, and A. Widera, A quantum heat engine driven by atomic collisions, *Nat. Commun.* **12**, 2063 (2021).
- [27] P. Talkner, M. Campisi, and P. Hänggi, Fluctuation theorems in driven open quantum systems, *J. Stat. Mech.* (2009) P02025.
- [28] M. Campisi, P. Talkner, and P. Hänggi, Fluctuation Theorems for Continuously Monitored Quantum Fluxes, *Phys. Rev. Lett.* **105**, 140601 (2010).
- [29] J. M. Horowitz, Quantum-trajectory approach to the stochastic thermodynamics of a forced harmonic oscillator, *Phys. Rev. E* **85**, 031110 (2012).
- [30] R. Kosloff and Y. Rezek, The quantum harmonic otto cycle, *Entropy* **19**, 136 (2017).
- [31] M. Izadyari, M. Öncü, K. Durak, and Ö. E. Müstecaplıoğlu, Quantum signatures in a quadratic optomechanical heat engine with an atom in a tapered trap, *J. Opt. Soc. Am. B* **39**, 3247 (2022).
- [32] F. Altintas and Ö. E. Müstecaplıoğlu, General formalism of local thermodynamics with an example: Quantum otto engine with a spin-1/2 coupled to an arbitrary spin, *Phys. Rev. E* **92**, 022142 (2015).
- [33] V. Singh, S. Singh, O. Abah, and Ö. E. Müstecaplıoğlu, Unified trade-off optimization of quantum harmonic otto engine and refrigerator, *Phys. Rev. E* **106**, 024137 (2022).
- [34] H. E. D. Scovil and E. O. Schulz-DuBois, Three-Level Masers as Heat Engines, *Phys. Rev. Lett.* **2**, 262 (1959).
- [35] M. O. Scully, K. R. Chapin, K. E. Dorfman, M. B. Kim, and A. Svidzinsky, Quantum heat engine power can be increased by noise-induced coherence, *Proc. Natl. Acad. Sci. USA* **108**, 15097 (2011).
- [36] G. Thomas and R. S. Johal, Coupled quantum otto cycle, *Phys. Rev. E* **83**, 031135 (2011).
- [37] K. Zhang, F. Bariani, and P. Meystre, Quantum Optomechanical Heat Engine, *Phys. Rev. Lett.* **112**, 150602 (2014).
- [38] A. Insinga, B. Andresen, and P. Salamon, Thermodynamical analysis of a quantum heat engine based on harmonic oscillators, *Phys. Rev. E* **94**, 012119 (2016).
- [39] M. T. Naseem and Ö. E. Müstecaplıoğlu, Quantum heat engine with a quadratically coupled optomechanical system, *J. Opt. Soc. Am. B* **36**, 3000 (2019).
- [40] J.-W. Zhang, J.-Q. Zhang, G.-Y. Ding, J.-C. Li, J.-T. Bu, B. Wang, L.-L. Yan, S.-L. Su, L. Chen, F. Nori, Ş K. Özdemir, F. Zhou, H. Jing, and M. Feng, Dynamical control of quantum heat engines using exceptional points, *Nat. Commun.* **13**, 6225 (2022).
- [41] M. A. Fox and J. K. Whitesell, *Organic Chemistry* (Jones and Bartlett, Burlington, MA, 1974).
- [42] R. G. Woolley, Quantum theory and molecular structure, *Adv. Phys.* **25**, 27 (1976).
- [43] Y. Saito and H. Hyuga, Colloquium: Homochirality: Symmetry breaking in systems driven far from equilibrium, *Rev. Mod. Phys.* **85**, 603 (2013).
- [44] J. Gal, The discovery of stereoselectivity at biological receptors: Arnaldo piutti and the taste of the asparagine enantiomers history and analysis on the 125th anniversary, *Chirality* **24**, 959 (2012).
- [45] E. J. Ariëns, Stereochemistry: A source of problems in medicinal chemistry, *Med. Res. Rev.* **6**, 451 (1986).
- [46] M. Quack and J. Stohner, Influence of Parity Violating Weak Nuclear Potentials on Vibrational and Rotational Frequencies in Chiral Molecules, *Phys. Rev. Lett.* **84**, 3807 (2000).
- [47] A. J. Hutt and S. C. Tan, Drug chirality and its clinical significance, *Drugs* **52**, 1 (1996).
- [48] Y.-Y. Chen, J.-J. Cheng, C. Ye, and Y. Li, Enantiodetection of cyclic three-level chiral molecules in a driven cavity, *Phys. Rev. Res.* **4**, 013100 (2022).
- [49] C. Ye, Y. Sun, and X. Zhang, Entanglement-assisted quantum chiral spectroscopy, *J. Phys. Chem. Lett.* **12**, 8591 (2021).
- [50] R. K. Kondru, P. Wipf, and D. N. Beratan, Atomic contributions

- to the optical rotation angle as a quantitative probe of molecular chirality, *Science* **282**, 2247 (1998).
- [51] R. Bielski and M. Tencer, Absolute enantioselective separation: Optical activity ex machina, *J. Sep. Science* **28**, 2325 (2005).
- [52] C. Ye, Q. Zhang, Y.-Y. Chen, and Y. Li, Determination of enantiomeric excess with chirality-dependent ac stark effects in cyclic three-level models, *Phys. Rev. A* **100**, 033411 (2019).
- [53] R. McKendry, M.-E. Theoclitou, T. Rayment, and C. Abell, Chiral discrimination by chemical force microscopy, *Nature (London)* **391**, 566 (1998).
- [54] R. Bielski and M. Tencer, A possible path to the rna world: Enantioselective and diastereoselective purification of ribose, *Orig Life Evol Biosph* **37**, 167 (2007).
- [55] P. Král and M. Shapiro, Cyclic Population Transfer in Quantum Systems with Broken Symmetry, *Phys. Rev. Lett.* **87**, 183002 (2001).
- [56] C. Ye, Q. Zhang, and Y. Li, Real single-loop cyclic three-level configuration of chiral molecules, *Phys. Rev. A* **98**, 063401 (2018).
- [57] J. Q. You and F. Nori, Atomic physics and quantum optics using superconducting circuits, *Nature (London)* **474**, 589 (2011).
- [58] M. Shapiro and P. Brumer, Controlled photon induced symmetry breaking: Chiral molecular products from achiral precursors, *J. Chem. Phys.* **95**, 8658 (1991).
- [59] M. Shapiro, E. Frishman, and P. Brumer, Coherently Controlled Asymmetric Synthesis with Achiral Light, *Phys. Rev. Lett.* **84**, 1669 (2000).
- [60] X. Li and M. Shapiro, Theory of the optical spatial separation of racemic mixtures of chiral molecules, *J. Chem. Phys.* **132**, 194315 (2010).
- [61] W. Z. Jia and L. F. Wei, Probing molecular chirality by coherent optical absorption spectra, *Phys. Rev. A* **84**, 053849 (2011).
- [62] D. Patterson, M. Schnell, and J. M. Doyle, Enantiomer-specific detection of chiral molecules via microwave spectroscopy, *Nature (London)* **497**, 475 (2013).
- [63] D. Patterson and J. M. Doyle, Sensitive Chiral Analysis via Microwave Three-Wave Mixing, *Phys. Rev. Lett.* **111**, 023008 (2013).
- [64] T. P. Orlando, J. E. Mooij, L. Tian, C. H. van der Wal, L. S. Levitov, S. Lloyd, and J. J. Mazo, Superconducting persistent-current qubit, *Phys. Rev. B* **60**, 15398 (1999).
- [65] T. T. Hönigl-Decrinis, I. V. Antonov, R. Shaikhaidarov, V. N. Antonov, A. Yu. Dmitriev, and O. V. Astafiev, Mixing of coherent waves in a single three-level artificial atom, *Phys. Rev. A* **98**, 041801(R) (2018).
- [66] Y. Guo, X. Gong, S. Ma, and C.-C. Shu, Cyclic three-level-pulse-area theorem for enantioselective state transfer of chiral molecules, *Phys. Rev. A* **105**, 013102 (2022).
- [67] M. Leibscher, T. F. Giesen, and C. P. Koch, Principles of enantio-selective excitation in three-wave mixing spectroscopy of chiral molecules, *J. Chem. Phys.* **151**, 014302 (2019).
- [68] C. H. Townes and A. L. Schawlow, *Microwave Spectroscopy* (Dover, New York, 1975).
- [69] S. Lobsiger, C. Perez, L. Evangelisti, K. K. Lehmann, and B. H. Pate, Molecular structure and chirality detection by fourier transform microwave spectroscopy, *J. Phys. Chem. Lett.* **6**, 196 (2015).
- [70] S. Eibenberger, J. Doyle, and D. Patterson, Enantiomer-Specific State Transfer of Chiral Molecules, *Phys. Rev. Lett.* **118**, 123002 (2017).
- [71] S. R. Domingos, C. Pérez, and M. Schnell, Sensing chirality with rotational spectroscopy, *Ann. Rev. Phys. Chem.*, **69**, 499 (2018).
- [72] H. T. Quan, Y. D. Wang, Y.-xi Liu, C. P. Sun, and F. Nori, Maxwell's Demon Assisted Thermodynamic Cycle in Superconducting Quantum Circuits, *Phys. Rev. Lett.* **97**, 180402 (2006).
- [73] See Supplemental Material at <http://link.aps.org/supplemental/10.1103/PhysRevE.107.L042103> for further details, which includes Refs. [74–78].
- [74] G. P. Hildred, S. S. Hassan, R. R. Puri, and R. K. Bullough, Thermal reservoir effects in resonance fluorescence, *J. Phys. B: At. Mol. Phys.* **16**, 1703 (1983).
- [75] H.-P. Breuer and F. Petruccione, *The Theory of Open Quantum Systems* (Oxford University Press, New York, 2007).
- [76] M. O. Scully and M. S. Zubairy, *Quantum Optics* (Cambridge University Press, Cambridge, England, 1997).
- [77] J. M. Fink, L. Steffen, P. Studer, L. S. Bishop, M. Baur, R. Bianchetti, D. Bozyigit, C. Lang, S. Filipp, P. J. Leek, and A. Wallraff, Quantum-To-Classical Transition in Cavity Quantum Electrodynamics, *Phys. Rev. Lett.* **105**, 163601 (2010).
- [78] J. R. Johansson, P. D. Nation, and F. Nori, Qutip 2: A python framework for the dynamics of open quantum systems, *Comput. Phys. Commun.* **184**, 1234 (2013).
- [79] H. T. Quan, Quantum thermodynamic cycles and quantum heat engines. ii, *Phys. Rev. E* **79**, 041129 (2009).
- [80] B. Leggio and M. Antezza, Otto engine beyond its standard quantum limit, *Phys. Rev. E* **93**, 022122 (2016).
- [81] J.-Q. Liao, H. Dong, X. G. Wang, X. F. Liu, and C. P. Sun, Spontaneous symmetry breaking in thermalization and anti-thermalization, [arXiv:0909.1230](https://arxiv.org/abs/0909.1230).
- [82] R. Dorner, S. R. Clark, L. Heaney, R. Fazio, J. Goold, and V. Vedral, Extracting Quantum Work Statistics and Fluctuation Theorems by Single-Qubit Interferometry, *Phys. Rev. Lett.* **110**, 230601 (2013).
- [83] L. Mazzola, G. De Chiara, and M. Paternostro, Measuring the Characteristic Function of the Work Distribution, *Phys. Rev. Lett.* **110**, 230602 (2013).
- [84] P. Talkner, E. Lutz, and P. Hanggi, Fluctuation theorems: Work is not an observable, *Phys. Rev. E* **75**, 050102(R) (2007).
- [85] A. Solfanelli, M. Falsetti, and M. Campisi, Nonadiabatic single-qubit quantum otto engine, *Phys. Rev. B* **101**, 054513 (2020).
- [86] M. Quack, On the measurement of the parity violating energy difference between enantiomers, *Chem. Phys. Lett.* **132**, 147 (1986).
- [87] C. Fábri, L. Horný, and M. Quack, Tunneling and parity violation in trisulfane (HSSH): An almost ideal molecule for detecting parity violation in chiral molecules, *ChemPhysChem* **16**, 3584 (2015).